

## Analytical solutions for crack opening displacements of eccentric cracks in thin-walled metallic plates

Wang, Wandong; Rans, Calvin; Benedictus, Rinze

**DOI**

[10.1016/j.tws.2017.11.047](https://doi.org/10.1016/j.tws.2017.11.047)

**Publication date**

2018

**Document Version**

Accepted author manuscript

**Published in**

Thin-Walled Structures

**Citation (APA)**

Wang, W., Rans, C., & Benedictus, R. (2018). Analytical solutions for crack opening displacements of eccentric cracks in thin-walled metallic plates. *Thin-Walled Structures*, 123, 371-381.  
<https://doi.org/10.1016/j.tws.2017.11.047>

**Important note**

To cite this publication, please use the final published version (if applicable).  
Please check the document version above.

**Copyright**

Other than for strictly personal use, it is not permitted to download, forward or distribute the text or part of it, without the consent of the author(s) and/or copyright holder(s), unless the work is under an open content license such as Creative Commons.

**Takedown policy**

Please contact us and provide details if you believe this document breaches copyrights.  
We will remove access to the work immediately and investigate your claim.

# Analytical solutions for crack opening displacements of eccentric cracks in thin-walled metallic plates

Wandong Wang<sup>a,\*</sup>, Calvin Rans<sup>a</sup>, Rinze Benedictus<sup>a</sup>

<sup>a</sup>*Structural Integrity & Composites Group, Faculty of Aerospace Engineering, Delft University of Technology, P.O. Box 5058, 2600 GB Delft, The Netherlands*

5

---

## Abstract

In the context of the prevalence of thin-walled metallic aerospace structures, the added resistance to crack propagation offered by a built-up structure is desirable from a damage tolerance standpoint. The analysis of failure in such structures, however, is limited by the lack of crack opening solutions. This paper develops analytical models that calculate crack opening displacements (CODs) for a more general cracking scenario, i.e. non-symmetric cracks. The proposed models are based on the Westergaard stress functions. It is then found that the COD solution of one model is particularly accurate. The potential significance of the obtained solutions lies in analysing failure in built-up structures containing non-symmetric cracks. The crack opening solution is particularly useful in estimating the load transfer between cracked body and intact bridging structures in built-up structures using the principle of displacement compatibility.

*Keywords:* Eccentric crack, crack opening displacement, stress intensity factor, load redistribution, Westergaard stress distribution

---

## 1. Introduction

10 Built-up structures with redundant load paths offer the ability to exploit and tailor progressive failure modes within these structures. This concept is often exploited in safety critical structures within the aerospace industry where damage arresting features, such as fuselage tear straps, and inherent redundant load paths in a given structure are used to slow damage progression and enable its detection through regular inspection the Damage Tolerance philosophy [1–5]. A major key to implementing the damage  
15 tolerance philosophy is the ability to predict damage growth behaviour. The period in which damage can grow without leading to catastrophic failure defines the available inspection intervals to detect the damage. However, predicting damage growth in redundant structures requires the ability to assess the impact of the damage on the stiffness of structural elements in order to effectively determine the load redistribution using solid mechanics and the concept of displacement compatibility [6].

20 The classical method for analyzing crack growth in many engineering materials is using linear elastic fracture mechanics (LEFM). In this approach, a linear elastic strain field is assumed in a continuum containing a crack, and this assumption is used to determine a compatible displacement field for a given load applied to the cracked body. Of primary interest for damage progression calculations is the magnitude of the singularity of the linear elastic stress field at the crack tip, or stress intensity factor ( $K$ ). Analytical  
25 solutions for the displacement field and stress intensity factor exist for a wide variety of crack configurations [7]. For crack configurations for which direct analytical solutions are not available, geometrical correction factors to modify the analytical solution for a crack in an infinite plate are often generated through experimental and/or numerical methods. These correction factors for stress intensity factor, known as  $\beta$  factors,

---

\*Corresponding author. Tel.: +31 (0)15 278 9748;  
E-mail address: w.wang-3@tudelft.nl

## Nomenclature

$a$	Half Crack length ( $mm$ )
$a_1$	Distance between maximum crack opening location and crack tip 1 ( $mm$ )
$a_2$	Distance between maximum crack opening location and crack tip 2 ( $mm$ )
$b$	Delamination ( $mm$ )
$d$	Distance between crack centre and panel centre ( $mm$ )
$d_1$	Distance between the location of $P_1$ and panel centre ( $mm$ )
$d_2$	Distance between the location of $P_2$ and panel centre ( $mm$ )
$e$	Eccentricity
$E$	Young's modulus ( $MPa$ )
$E_f$	Young's modulus of fibre layer ( $MPa$ )
$K$	Stress intensity factor ( $MPa\sqrt{mm}$ )
$K_{br}$	Stress intensity factor for crack tip 2 ( $MPa\sqrt{mm}$ )
$K_{total}$	Total stress intensity factor of the metal layer in Glare panels ( $MPa\sqrt{mm}$ )
$L$	Distance from crack tip to the free edge ahead ( $mm$ )
$P$	Integral of stress distribution in front of crack tip ( $N$ )
$P_{app}$	Total applied load ( $N$ )
$S_{br}$	Bridging stress distribution $MPa$
$S_f$	Stress in the fibre layer due to applied load $MPa$
$S_m$	Stress in the metal layer due to applied load $MPa$
$t$	Thickness ( $mm$ )
$w$	Distance between crack datum and free edge ( $mm$ )
$W$	Panel width ( $mm$ )
$x$	Horizontal location in a xy-coordinate system ( $mm$ )
$x_c$	Centroid of the stress distribution in front of the crack tip ( $mm$ )
$y$	Vertical location in a xy-coordinate system ( $mm$ )
$\sigma$	Applied tensile stress ( $MPa$ )
$\sigma_{yy}$	Stress distribution in front of crack tip in loading direction ( $MPa$ )
$\tau_{xy}$	shear stress ( $MPa$ )
$\lambda$	Normalized crack length
$\beta$	Correction factor for stress intensity factor
$\beta_{Isida}$	Correction factor for stress intensity factor derived by Isida
$v$	Crack opening displacement ( $mm$ )
$v_{ff}$	Crack opening displacement due to far-field stress ( $mm$ )
$v_{br}$	Crack opening displacement due to bridging stress ( $mm$ )
$\delta_f$	Fibre elongation ( $mm$ )
subscripts:	
1	referring to crack tip 1
2	referring to crack tip 2

are widely available in the literature [7–12]. However, corrections for the displacement field are often not available.

The accuracy of  $\beta$  factors developed by Isida is better than 1% [7]. The  $\beta$  factors were developed by expressing the Airy's stress functions in terms of complex potential functions and solving these potential functions [12]. The  $\beta$  factors are expressed as functions of the coefficients which are tabulated in [12]. However, the accurate  $\beta$  factors cannot be directly applied for an eccentrically cracked panel containing stiffening elements. The interplay between the eccentrically cracked panel and the redundant load paths must be taken into consideration in calculating the stress singularity in front of the crack tips.

The objective of this paper is to develop means of correcting the Mode I crack opening displacement (COD) of non-symmetric cracks in thin-walled metallic panels using linear elastic fracture mechanics. The inherent assumptions of LEFM have to be respected when applying the developed approach. The proposed approach is envisioned to be applicable to thick panels where the state of plane strain is valid.

The purpose of developing such correcting methods is to assist the analysis of failure in eccentrically cracked panels with stiffening elements. This paper proposes 4 analytical models based on the Westergaard stress function [13]. The Westergaard stress function is simplified to provide solutions for the crack opening displacement and stress-strain field ahead of a non-symmetric crack. The stress intensity factor solutions

45 arising from the simplified Westergaard stress function are compared to the results of Isida to show the validity of the proposed models. A validated Finite Element Modeling (FEM) technique is applied to obtain the COD and strain field in front of non-symmetric cracks, the simulation results are used to screen the 4 models in section 4. In section 5, the opening displacement solution will be employed in a simplified case study to evaluate the impact of the load transfer mechanism on the stress intensity factors.

## 50 2. The Westergaard function method

The Westergaard function method is a very convenient methodology to characterize the entire stress and strain fields for a cracked body. The Westergaard functions can also be simplified to their near-tip solutions, i.e. stress intensity factor (SIF) solutions which provide the stress and strain distributions at the crack tip vicinities [7, 14]. In some instances, however, it is desirable to know the entire stress-strain field ahead of the crack tip. Load redistribution due to stiffness variation (either geometric or material stiffness) can be resolved from such a stress-strain field, such as the analysis of crack growth behaviour in a stiffened panel conducted by Rans [6].

The closed-form Westergaard solutions are strictly applicable to infinite plate crack problems except for Mode III crack problems [7]; nevertheless they can be modified to provide meaningful solutions for a finite panel with a crack [6, 15, 16]. Barsoum et al. [15, 16] predict the stress intensity factor for cracks in finite width functionally graded material containing layers with different stiffness using this method. With the same assumption, Rans [6] predicts the crack growth in stiffened metallic panels.

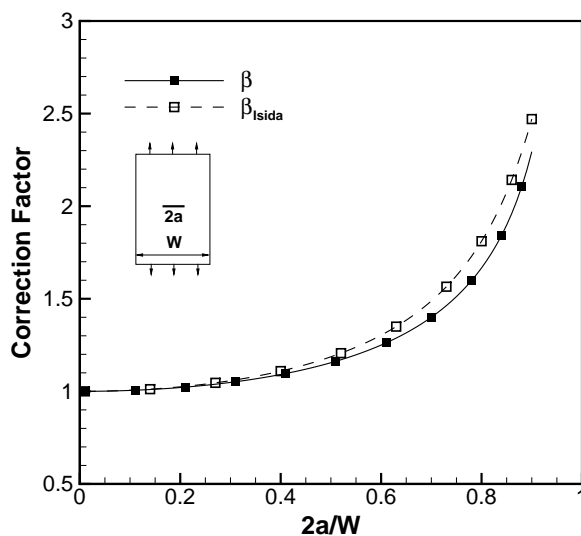


Figure 1: Comparison of correction factors for a central crack in finite panel

Consider a central crack embedded in a finite panel under uniform tensile loading, a Mode I crack problem, the stress ahead of the crack tip along crack plane can be assumed to follow the Westergaard stress distribution [7, 11]:

$$\sigma_{yy} = \frac{\sigma \cdot \beta}{\sqrt{1 - (a/x)^2}} \quad (1)$$

where  $\sigma$  is applied stress,  $\beta$  is a correction factor,  $a$  is the crack length and  $x$  the distance from the crack centre in the crack plane.

The introduction of the correction factor  $\beta$  is to account for the influence of the finite width boundary condition. The correction factor  $\beta$  is a function of crack length and panel width. This variable can be

calculated using the load equilibrium between the crack section and far-field. For a finite panel of width  $W$ , the load equilibrium can be expressed as:

$$\sigma \cdot W = 2 \int_a^{W/2} \frac{\sigma \cdot \beta}{\sqrt{1 - (a/x)^2}} dx \quad (2)$$

Solving the integral for a uniform stress state and rearranging for  $\beta$ :

$$\beta = \frac{1}{\sqrt{1 - (2a/W)^2}} \quad (3)$$

The corresponding crack opening displacement for plane stress state can be given by:

$$2v = \frac{4\beta\sigma}{E} \sqrt{a^2 - x^2} \quad (4)$$

and stress intensity factor is expressed as following:

$$K = \beta\sigma\sqrt{\pi a} \quad (5)$$

The correction factor  $\beta$  is plotted in Fig.1 against the ratio between the crack length and specimen width. In order to show the validity of the solution from the simplified Westergaard stress function, the obtained correction factor for SIF is compared to that derived by Isida. see Fig.1. Good correlation can be observed.

It is worth noting that a finite panel with a central crack under Mode I loading possesses a symmetric axis passing through the crack centre in loading direction. The Westergaard stress distributions in front of two crack tips, crack opening displacement configuration are symmetric with respect to this symmetric axis (or crack centre). Especially it can be seen in Eqs. (1, 4, 5) that these variables are functions of the crack length  $a$  which is measured from the crack centre, also the location of maximum crack opening, to the crack tip.

The presence of an eccentric crack in a finite panel under Mode I loading eliminates the symmetric condition possessed by a centrally cracked panel. As a result, the COD configuration and the stress distributions (stress-strain fields) ahead of the non-symmetric crack tips are expected to be asymmetric with respect to its crack centre. The analysis of this non-symmetric deformation behaviour in an eccentrically cracked panel is detailed in the following section.

### 3. Models for calculating the COD of a non-symmetric crack

The generalized approach for modelling the COD of a non-symmetric crack is as follows. First, it is assumed that the Westergaard stress distribution (Eq. 1) and associated COD solution (Eq. 4) are applicable to both crack tips in the non-symmetric crack. Due to the non-symmetry, a different magnitude of the Westergaard stress distribution is expected in front of each crack tip as illustrated by the difference in  $\sigma_{yy,1}$  and  $\sigma_{yy,2}$  in Fig. 2. This difference can be captured by a difference in the  $\beta$  factor for each crack tip. These  $\beta$  factors are obtained by integrating the Westergaard stress distribution and equating it to the applied load.

In applying this generalized approach, assumptions need to be made regarding the definition of crack length and the load distribution in the cracked panel. When defining the half-crack lengths, one needs to keep in mind that the COD solution arising from the Westergaard stress distribution describes a half crack with a maximum displacement at the root of the crack ( $x = 0$ ). Thus, the definition of the datum for measuring the crack length artificially prescribes the point of maximum COD for the crack. Load redistribution is also a key factor to consider. The presence of a crack changes the stiffness of a panel and can cause load to be preferentially carried by one or the other sides of the panel. This affects the load equilibrium expressed in Eq. 2. Three different cases were considered which are all illustrated in Fig. 3. These 3 models generate the COD and  $\beta$  factors. An additional model based on known  $\beta$  factors is also developed to back derive the COD solution.

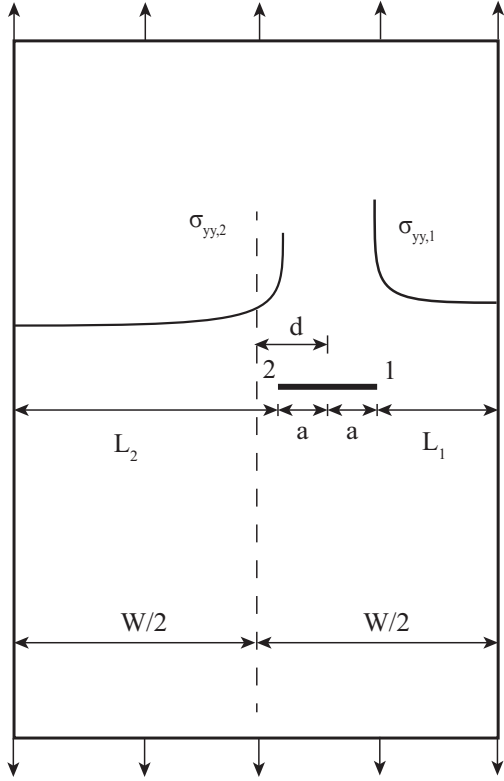


Figure 2: Illustration of eccentric crack configuration and different stress distributions in front of two crack tips

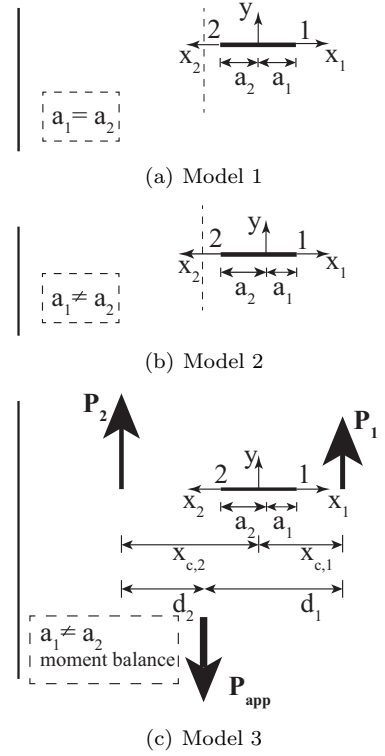


Figure 3: Comparison of the 3 models

In Model 1, the datum for the crack length definition is assumed to be in the centre of the crack ( $a_1 = a_2$ ) and the resultant of the Westergaard stress distribution is assumed to be equal to the applied load acting over the half-width of the panel defined from the crack datum (i.e., no load redistribution in the panel). This is illustrated in Fig. 3(a). A consequence of the assumed crack datum is that the maximum COD will occur in the centre of the crack, and due to the difference in  $\beta$  for each crack tip, there will be a discontinuity in COD at this point. Besides, the variation in SIF is a result of the reduction of the net-section of the panel in the crack plane alone.

In Model 2, the presence of the discontinuity of COD in Model 1 is corrected. The datum for the crack length definition is allowed to deviate from the centre of the crack such that the COD of both cracks are equal at the crack datum. This is illustrated in Fig. 3(b). Assumptions regarding the load distribution remain the same as in Model 1.

In Model 3, the possibility of load redistribution is examined. If the boundary conditions for loading do not provide rotational constraint (i.e., a pin-clevis connection), the resultant load on either side of the crack will redistribute to maintain moment equilibrium in the panel as illustrated in Fig. 3(c). This load redistribution case is considered in this model with the same crack datum definition procedure as Model 2.

Finally, the last model based on back calculating the known Isida  $\beta$  factors is proposed. The load redistribution in this case is assumed to cause the two different Westergaard stress distributions to have the same stress intensity factors described by Isida. The crack datum definition of Model 2 is also considered in this model.

The eccentricity convention in [12] is used in this paper to define the location of a non-symmetric crack. As illustrated in Fig. 2, the width of the panel is  $W$  and the total crack length is denoted as  $2a$ . The distance

from crack centre to the centre of the panel is  $d$ . Then the eccentricity,  $e$ , is defined as:

$$e = 2d/W \quad (6)$$

The distances from crack tip 1 and 2 to their corresponding edges ahead (Fig. 2) can be calculated:

$$L_1 = \frac{W}{2}(1 - e) - a \quad (7)$$

$$L_2 = \frac{W}{2}(1 + e) - a \quad (8)$$

Then the normalized crack length is given as:

$$\lambda = \frac{a}{L_1 + a} \quad (9)$$

### 3.1. Model 1: symmetric crack lengths definition and load equilibrium method

As shown in Fig. 2, one eccentric crack is embedded in a panel under far-field tensile loading. For this model, the crack length,  $a$ , is defined as the length from the crack centre to the crack tip ( $a_1 = a_2$  in Fig. 3(a)). The stress distributions in front of the crack tips are then given as the Westergaard stress distribution respectively:

$$\sigma_{yy,1} = \frac{\sigma \cdot \beta_1}{\sqrt{1 - (a/x_1)^2}} \quad (10)$$

$$\sigma_{yy,2} = \frac{\sigma \cdot \beta_2}{\sqrt{1 - (a/x_2)^2}} \quad (11)$$

where  $x$  is the distance from the crack centre.

Integrations of the stress distributions give the loads carried by the uncracked material in front of the crack tips respectively:

$$P_1 = \int_a^{w_1} \sigma_{yy,1} dx_1 \cdot t \quad (12)$$

$$P_2 = \int_a^{w_2} \sigma_{yy,2} dx_2 \cdot t \quad (13)$$

where  $w_1 = L_1 + a$  and  $w_2 = L_2 + a$  and  $t$  denotes the thickness of the panel.

For this model, this load equilibrium between the crack section and far-field is implemented in the following way:

$$P_1 = \sigma \cdot w_1 \cdot t \quad (14)$$

$$P_2 = \sigma \cdot w_2 \cdot t \quad (15)$$

This means of implementing load equilibrium assumes no load redistribution in two half-width panels defined by the crack datum in this model. From Eqs. (10 –15), the correction factors  $\beta_1$  and  $\beta_2$  can be easily determined:

$$\beta_1 = \frac{1}{\sqrt{1 - (a/w_1)^2}} \quad (16)$$

$$\beta_2 = \frac{1}{\sqrt{1 - (a/w_2)^2}} \quad (17)$$

The crack opening displacements can also be calculated according to the Westergaard method. The opening configuration of the half crack for tip 1 is given:

$$2v_1 = \frac{4\beta_1\sigma}{E} \sqrt{a^2 - x_1^2} \quad (18)$$

and that of the crack tip 2 is given by:

$$2v_2 = \frac{4\beta_2\sigma}{E}\sqrt{a^2 - x_2^2} \quad (19)$$

Then it becomes obvious that the calculated maximum crack opening displacements at  $x_1 = x_2 = 0$  are not identical for an eccentric crack, which violates the physics of this crack problem. It is then concluded that Model 1 cannot be used to calculate the crack opening displacement configuration for a non-symmetric crack. The analysis process proves that the definition of crack datum at the crack centre can lead to the computed displacement incompatibility. In other words, the maximum crack opening location is not the crack centre for non-symmetric cracks.

According to the analysis in Section 2,  $\beta_1$  and  $\beta_2$  are also correction factors for the stress intensity factors of the two crack tips respectively.

In Fig. 4, the calculated correction factors together with Isida's results are plotted against normalized crack length,  $\lambda$ , for several typical eccentricities to show the accuracy of stress intensity factors arising from this model. For crack tip 1, the  $\beta_1$  curves calculated with the proposed Model 1 overlap with each other for all eccentricities. It can be observed that the predicted results correlate with Isida's prediction results decently. However, the correction factors for crack tip 2 are underestimated for all eccentricities. Especially for eccentricities larger than 0.6, the predicted results almost keep constant with crack length. This probably can be attributed to the fact that the influence of the boundary ahead of crack tip 1 on crack tip 2 is neglected.

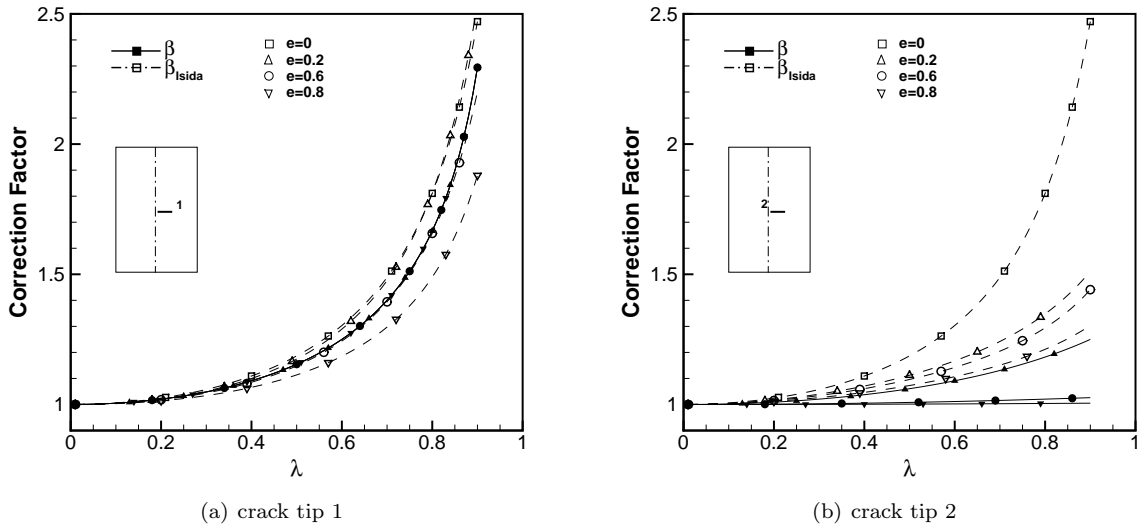


Figure 4: Correction factors comparison of Model 1

### 3.2. Model 2: non-symmetric crack lengths definition and load equilibrium method

The definition of the crack length,  $a$ , in Model 1 leads to the displacement incompatibility at the location of crack centre. It is therefore reasonable to deviate the maximum crack opening location from the centre. The location of the maximum crack opening is still an unknown parameter for a non-symmetric crack.

In this model, the total crack length is given as  $2a$  and two crack lengths  $a_1$  and  $a_2$  are the lengths between the location of maximum crack opening displacement and crack tip 1 and 2 respectively (see Fig. 3(b)). The sum of the two crack lengths is equal to the total crack length:

$$a_1 + a_2 = 2a \quad (20)$$

The Westergaard stress distributions in front of the crack tips are expressed as

$$\sigma_{yy,1} = \frac{\sigma_1}{\sqrt{1 - (a_1/x_1)^2}} \quad (21)$$

$$\sigma_{yy,2} = \frac{\sigma_2}{\sqrt{1 - (a_2/x_2)^2}} \quad (22)$$

where  $x_1$ ,  $x_2$  are from the maximum crack opening location (Fig. 3(b)) and  $\sigma_1$ ,  $\sigma_2$  are to be determined.

In this case, the loads carried by the uncracked material in front of the crack tips can be calculated in a similar way as Eqs.(12, 13):

$$P_1 = \int_{a_1}^{w_1} \sigma_{yy,1} dx_1 \cdot t \quad (23)$$

$$P_2 = \int_{a_2}^{w_2} \sigma_{yy,2} dx_2 \cdot t \quad (24)$$

140 but with  $w_1 = L_1 + a_1$  and  $w_2 = L_2 + a_2$ , denoting that  $w_1$  and  $w_2$  are the widths of two half-panels defined from the crack datum.

The load equilibrium is also implemented in a similar way as in Model 1:

$$P_1 = \sigma \cdot w_1 \cdot t \quad (25)$$

$$P_2 = \sigma \cdot w_2 \cdot t \quad (26)$$

It is notable that no load redistributes between the two half-width panels defined by the crack datum in this model either. The crack datum definition in this model prescribes two different half-width panels compared to Model 1.

Furthermore, the maximum crack opening displacement should be equal for the two half cracks at  $x_1 = x_2 = 0$ , which can be expressed as:

$$\frac{4\sigma_1}{E} \sqrt{a_1^2 - 0^2} = \frac{4\sigma_2}{E} \sqrt{a_2^2 - 0^2} \quad (27)$$

The system of Eqs. (20 - 27) can be simplified into a non-linear function of  $a_1$ . Analytically solving such a non-linear could be difficult. A combination of bisection, secant and inverse quadratic interpolation methods is applied to solve for  $a_1$  numerically. All other unknown variables can then be easily calculated. The COD for each half crack length is then expressed as following respectively:

$$v_1 = \frac{2\sigma_1}{E} \sqrt{a_1^2 - x_1^2} \quad (28)$$

$$v_2 = \frac{2\sigma_2}{E} \sqrt{a_2^2 - x_2^2} \quad (29)$$

The SIF solutions for the two crack tips can be expressed as following:

$$K_1 = \sigma_1 \sqrt{\pi a_1} \quad (30)$$

$$K_2 = \sigma_2 \sqrt{\pi a_2} \quad (31)$$

In order to compare with Isida's prediction, the correction factors are calculated as:

$$\beta_1 = \frac{K_1}{\sigma \sqrt{\pi a}} = \frac{\sigma_1 \sqrt{\pi a_1}}{\sigma \sqrt{\pi a}} \quad (32)$$

$$\beta_2 = \frac{K_2}{\sigma \sqrt{\pi a}} = \frac{\sigma_2 \sqrt{\pi a_2}}{\sigma \sqrt{\pi a}} \quad (33)$$

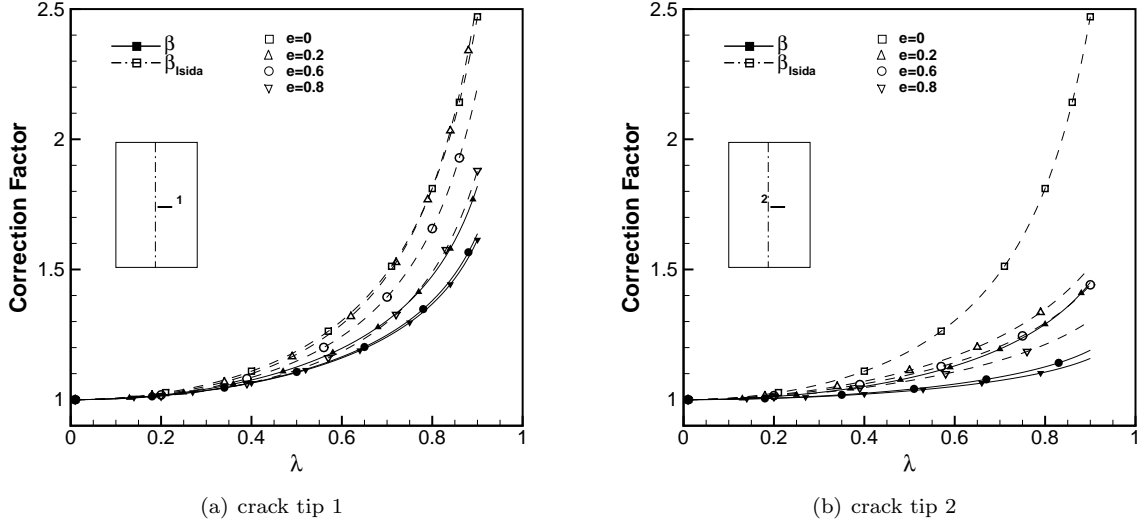


Figure 5: Correction factors comparison of Model 2

145 The comparison is given in Fig. (5). The predicted correction factors for crack tip 1 and 2 are both underestimated when the normalized crack length is larger than 0.4, especially for the prediction of crack tip 1.

150 In fact, the implementation of the load equilibrium in these two models does not consider the load redistribution due to the stiffness difference in both sides of an eccentrically cracked panel. The presence of a non-symmetric crack changes the stiffness of a panel and the load is preferentially carried by the one or the other sides of the panel. These effects of load redistribution are accounted for in Model 3.

### 3.3. Model 3: load equilibrium and moment equilibrium method

155 The possibility of load redistribution is examined in this model. The stress distributions in front of the crack tips are assumed as the same as in Model 2, i.e. Eqs.( 21, 22). The definition of crack datum remains the same. Crack displacement compatibility at maximum crack opening location is implemented as Eq. 27.

The loads carried by the material in front of crack tip 1 and crack tip 2 are given as Eqs. 23 and 24, the implementation of load equilibrium is expressed in following manner for this model:

$$P_1 + P_2 = P_{app} \quad (34)$$

with  $P_{app} = \sigma \cdot Wt$  being the total applied far-field load.

In addition, the load on either side of the crack,  $P_1$  and  $P_2$ , redistributes to maintain the moment equilibrium in the panel (Fig.3(c)).

The location of the equivalent load  $P_1$  for the stress distribution in front of crack tip 1 is the centroid of the distribution shape in its own coordinates.

$$x_{c,1} = \frac{\int_{a_1}^{w_1} \sigma_{yy,1} x_1 dx_1}{\int_{a_1}^{w_1} \sigma_{yy,1} dx_1} \quad (35)$$

and the location of the equivalent load  $P_2$  is

$$x_{c,2} = \frac{\int_{a_2}^{w_2} \sigma_{yy,2} x_2 dx_2}{\int_{a_2}^{w_2} \sigma_{yy,2} dx_2} \quad (36)$$

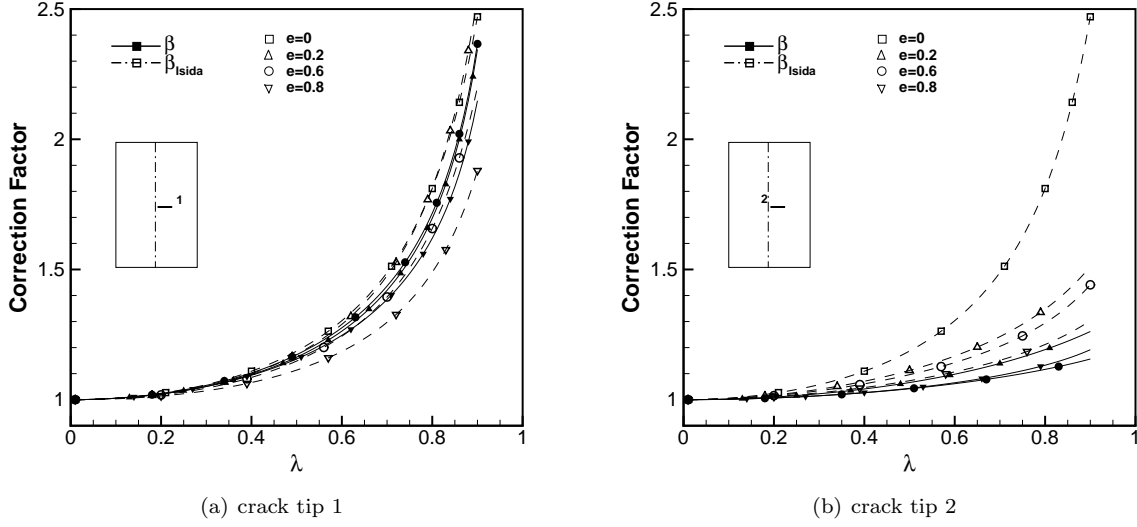


Figure 6: Correction factors comparison of Model 3

Then the mathematical description of the moment equilibrium is given as:

$$P_1 d_1 = P_2 d_2 \quad (37)$$

where  $d_1$  and  $d_2$  are distances from locations of  $P_1$  and  $P_2$  to the panel centre respectively (Fig. 3(c)) and are expressed as:

$$d_1 = a + d + x_{c,1} - a_1 \quad (38)$$

$$d_2 = a - d + x_{c,2} - a_2 \quad (39)$$

The same numerical solution in Model 2 is applied to obtain the values of all unknown variables. The opening displacements for two half crack lengths are given in the same manner as Eqs (28, 29). The correction factors are also given in the same way as Eqs. (32, 33). The comparison for some typical eccentricities and normalized crack lengths is made in Fig. 6.

From the comparison in Fig. 6, it can be seen that the correlation for crack tip 1 is very good for different eccentricities. For crack tip 2, the correction factors are underestimated for all the eccentricities. The error becomes larger as the crack length increases, especially for  $\lambda > 0.6$ . However, crack tip 1 is much more critical than crack tip 2. Accurate prediction of stress intensity factor for crack tip 1 is much more critical then. Besides, the proposed Model 3 should provide sufficiently accurate prediction results for practical structures in aircraft industry as the thin walled structures normally are very wide. The possibility of the appearance of an extreme crack configuration with both high eccentricity and high  $\lambda$  should be very low.

#### 3.4. Model 4: method of back calculating Isida $\beta$ factors

As can be seen, there are certain discrepancies between the  $\beta$  factors of the above 3 models and those of Isida. In this model, the Isida  $\beta$  factors are used. The datum for the crack length definition in Model 2 is applied in this model. It is assumed that the stress intensity factors due to the load redistribution should be equal to the ones given by Isida, which are expressed as:

$$\beta_1 \sigma \sqrt{\pi a} = \sigma_1 \sqrt{\pi a_1} \quad (40)$$

$$\beta_2 \sigma \sqrt{\pi a} = \sigma_2 \sqrt{\pi a_2} \quad (41)$$

It is obvious that Eq.(20) and Eq.(27) should be met in this model as well. The two half crack lengths can then be easily derived, which are given as:

$$a_1 = \frac{2a}{1 + \frac{\beta_1^2}{\beta_2^2}} \quad (42)$$

$$a_2 = \frac{2a}{1 + \frac{\beta_2^2}{\beta_1^2}} \quad (43)$$

The corresponding Wastergaard stress distributions in front the crack tips are

$$\sigma_{yy,1} = \frac{\beta_1 \sqrt{a} x_1}{\sqrt{a_1(x_1^2 - a_1^2)}} \quad (44)$$

$$\sigma_{yy,2} = \frac{\beta_2 \sqrt{a} x_2}{\sqrt{\pi a_2(x_2^2 - a_2^2)}} \quad (45)$$

and the crack opening displacements for the two half crack lengths are

$$v_1 = \frac{2\beta_1 \sigma \sqrt{a}}{E \sqrt{a_1}} \sqrt{a_1^2 - x_1^2} \quad (46)$$

$$v_2 = \frac{2\beta_2 \sigma \sqrt{a}}{E \sqrt{a_2}} \sqrt{a_2^2 - x_2^2} \quad (47)$$

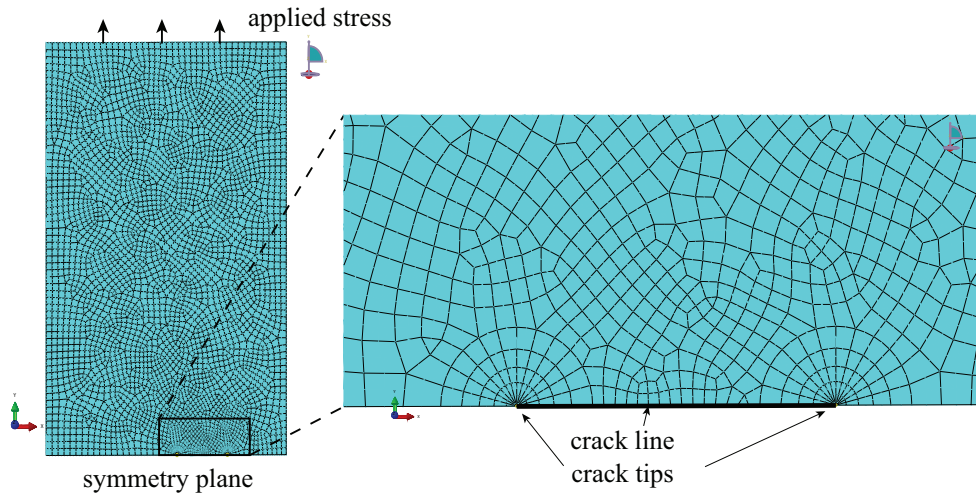


Figure 7: Mesh of the FEA model for an Al 2024-T3 panel with an eccentric crack

Table 1: Parameters used in FEA models

	Young's Modulus	Poission's Ratio	Thickness	Width	Length	Stress
Values	72400[MPa]	0.33	0.4[mm]	200[mm]	300[mm]	100[MPa]

## 4. Verification

The near tip solutions of the Westergaard stress distributions, SIF results, for eccentric cracks have been validated with the analytical results of Isida. Using FEM technique, the verification of the predicted deformation field of eccentrically cracked panels is carried out in this section. The crack opening displacement and stress-strain field in front of crack tips are of particular interest. Due to the fact that Model 1 is not able to predict a continuous crack opening displacement configuration for a non-symmetric crack, only the crack opening displacements predicted by the other 3 models are compared to FEM results. The Westergaard stress distributions and stress intensity factor results predicted by Model 2 and Model 3 are also compared to FEM results in order to present an intuitive validation of the usage of the Westergaard method.

### 4.1. Finite element analysis

The commercial FEM package ABAQUS was applied to numerically simulate the crack opening displacement, stress distributions in front of two crack tips and stress intensity factors for cracks in the eccentrically cracked metal panel with finite width. The FEA results are used to validate the results derived from the models proposed in section 3.

The studied case is a Al 2024 – T3 panel with the configuration and loading parameters given in Table 1. The material properties of Al 2024-T3 listed in Table 1 were used for the simulation. The metal panels were modelled using 3-D shell planar. Due to the symmetry of the problem, only the upper half of the panel was modelled. The bottom edge where the crack was defined was assigned the symmetry plane and the far-field stress was applied to the upper edge, see Fig. 7.

The J-integral evaluation technique was applied to calculate the stress intensity factors for the crack tips [17]. The number of contours was 5 and a square root singularity at the crack tip was used. The quadratic, reduced integration element *S8R5* elements were used to mesh the crack tip zone with the swept meshing technique. The element size around the crack tip is 0.1 mm. The rest of the body was meshed using the *S8R* elements and the free meshing technique. Fig. 7 shows the overall mesh and the local-mesh around the crack tip.

Four non-symmetric crack cases were studied. The total crack length for all the cases was 40 mm. The eccentricities were 0, 0.1, 0.5, 0.7 respectively.

### 4.2. Comparison

Firstly, the stress intensity factors for all the chosen cases are summarized in Table 2. As can be seen, the differences in the  $K$  values calculated with FEM and those of Isida are quite small for all the studied cases. It proves that the FEM simulation provides valid results. According to the comparison in Table 2, it shows again that Model 3 gives better prediction than Model 2.

Table 2: K values comparison

e		FEM	Isida	Model 2 (relative error %)	Model 3 (relative error %)
0	$K_1$	812.1	812.2	809.0 (-0.38)	809.0 (-0.38)
	$K_2$	812.1	812.2	809.0 (-0.38)	809.0 (-0.38)
0.1	$K_1$	814.5	814.6	811.2 (-0.40)	813.4 (-0.13)
	$K_2$	812.1	812.2	807.9 (-0.52)	806.3 (-0.71)
0.5	$K_1$	865.8	866.0	845.3 (-2.37)	874.5 (1.01)
	$K_2$	843.6	843.8	814.8 (-3.41)	813.6 (-3.56)
0.7	$K_1$	1024	1026.6	961.3 (-6.12)	1077.4 (5.21)
	$K_2$	919.5	920.5	847.9 (-7.78)	856.8 (-6.81)

In Fig. 8, the crack opening displacement comparisons between the FEM and the models are made.  $x = 0$  in the figure denotes crack tip 2 and  $x = 40$  indicates crack tip 1. The dashed vertical lines in Fig. 8 denote the analytically calculated maximum crack opening locations. As can be seen, the crack opening

for the case of  $e = 0.1$  is almost the same as the central crack. Predictions from Model 2 and Model 3 for eccentricities of 0 and 0.1 correlate with FEA results very well. It is interesting that the crack opening increases with increasing eccentricity for the same crack length. Both models captures this phenomenon, but Model 3 provides better prediction results. Model 4 provides the most accurate COD predictions for all the studied cases. The results of  $e = 0.5$  and  $e = 0.7$  prove that the datum for the crack length definition should deviate from the crack center for a non-symmetric crack.

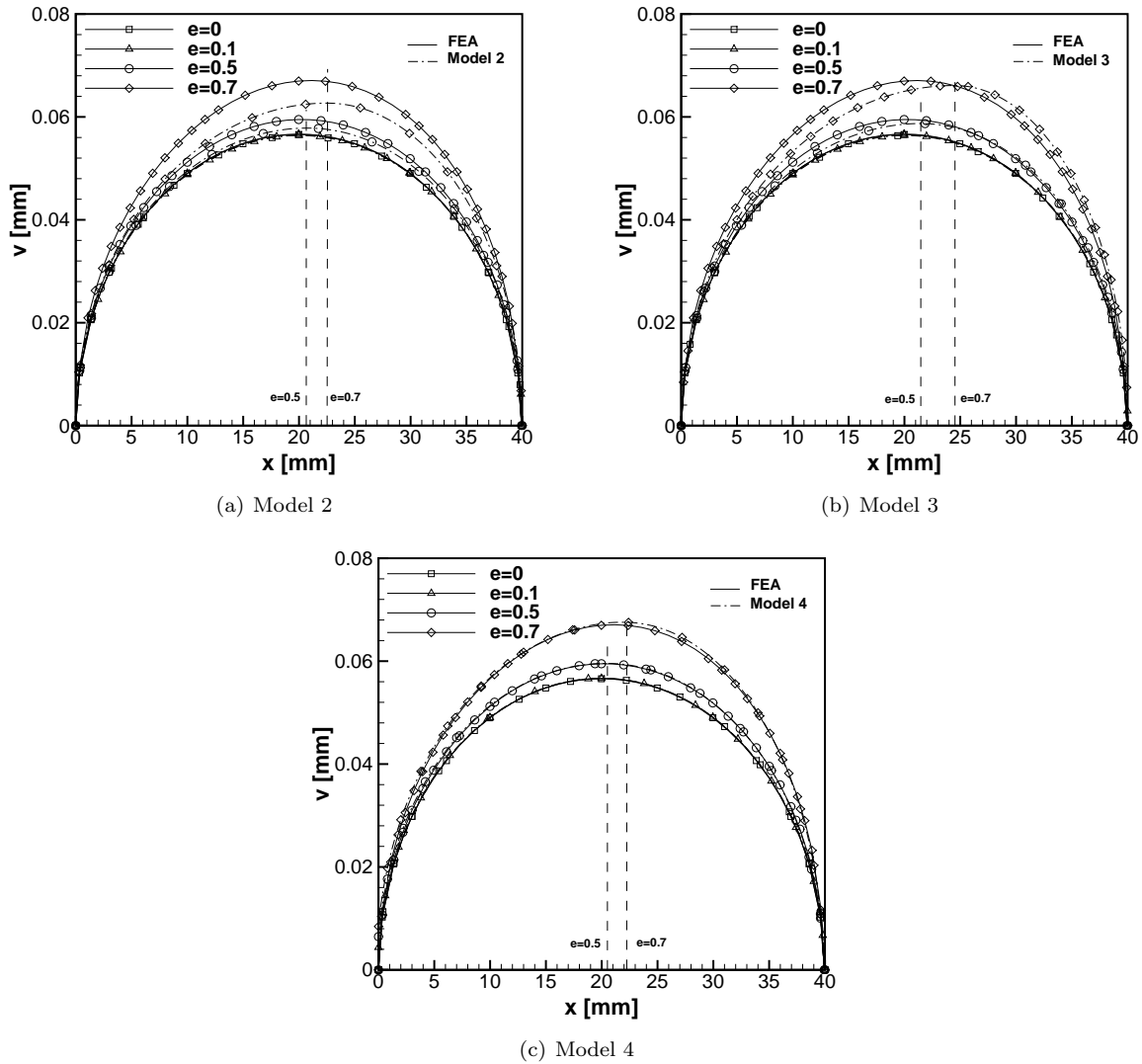


Figure 8: COD comparison

The predicted stress distributions in front of crack tips are also compared to FEA results to verify the assumption of the Westergaard stress distribution in front of the crack tips. This comparison for the case of  $e = 0.5$  is presented in Fig. 9. The points highlighted with dashed circles is due to the singularity at the node of a transition from a triangular element to a quadrilateral element (Fig. 7), i.e. a calculation error occurs at this node in front of the crack tip. Nevertheless the overall trend of stress distributions are the same. Only slight difference can be observed between Model 2 and Model 3 near the the crack tip.

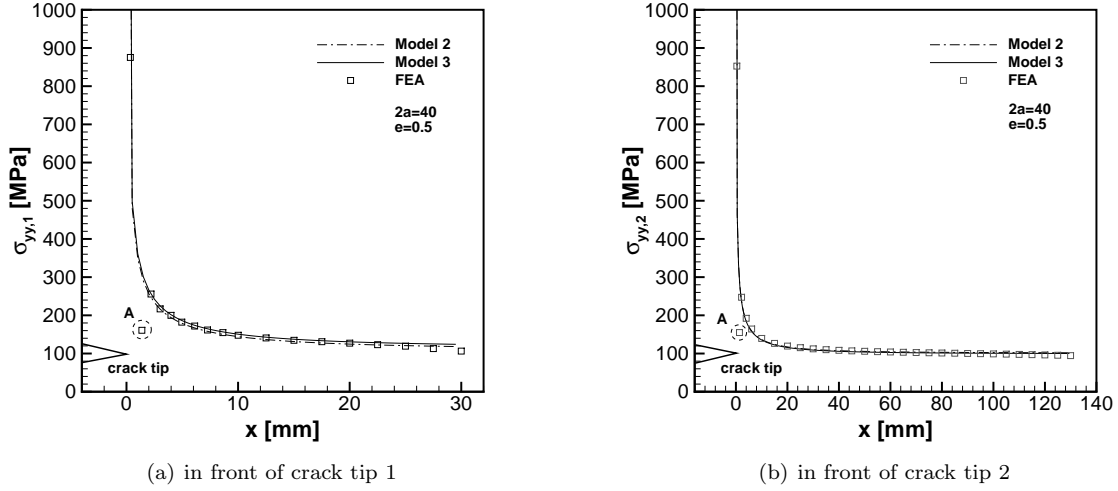


Figure 9: Stress distribution comparison

## 5. Discussion

The significance of predicting the displacement field lies in analysing the failure in built-up structures. The influence of stiffening elements on the stress intensify factors in a cracked panel can be estimated with the concept of displacement compatibility. An example of exploring the crack opening displacement of a non-symmetric crack in a stiffened aluminum panel is presented in this section to formulate this discussion.

### 5.1. A simplified example of using the COD solution for analysing failure in built-up structures

A glass-fibre reinforced aluminium panel, normally called Glare, is considered here. For simplicity, the considered panel is made of a 2024-T3 aluminium layer in the middle and two layers of S-2 glass fibres in loading direction bonded on both sides of the metal layer. Fatigue cracking in Glare has been extensively studied [5, 18]. It is well understood that the fatigue resistant fibres remain intact and bridge the crack in the metal layers, resulting in high resistance to fatigue cracking in such built-up panels. This bridging mechanism also causes delamination at the metal/composite interfaces. The well established calculation method of analysing the crack state and bridging mechanism in Glare developed by Alderliesten [5, 18] is simplified to demonstrate the significance of the COD solution for non-symmetric cracks.

For the purpose of this discussion, two damage status in the laminate shown in Fig. 10 are studied. Case 1 is a central crack and Case 2 is a non-symmetric crack of  $e = 0.5$ . The total crack length for both cases is  $2a = 40 \text{ mm}$  and the two cracks have the same delamination shape which is given by Eq. 48. The delamination shapes at both metal/composite interfaces are symmetric with respect to the aluminium layer in either case. The symmetric damage status of Case 1 provides a benchmark.

$$b(x) = 3\sqrt{1 - \frac{|x|}{a}} \quad (48)$$

The properties of the constituents used for this panel are provided in Table 3. The laminate is cured at a maximum pressure of 6 bars and a maximum temperature of 120 °C. 100 MPa tensile stress is applied on the panel.

The total stress intensity factor ( $K_{total}$ ) at the crack tip in the panel can be superposed by the stress intensity factor due to the far-field applied load ( $K$ ) and the stress intensity factor due to the bridging mechanism ( $K_{br}$ ) [5, 18].

Table 3: Material properties

	Al	Prepreg
Young's modulus $E_x$ [GPa]	72.4	48.9
Young's modulus $E_y$ [GPa]	72.4	5.5
Shear modulus $G_{xy}$ [GPa]	27.6	5.55
Poisson's ratio $\nu_{xy}$	0.33	0.33
Poisson's ratio $\nu_{yx}$	0.33	0.0371
Thickness of single layer [mm]	0.4	0.133
Width [mm]	200	200
Thermal expansion coefficient [1/°C]	$22 \cdot 10^{-6}$	$6.1 \cdot 10^{-6}$ (0°) $26.2 \cdot 10^{-6}$ (90°)

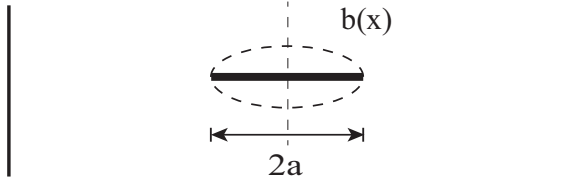
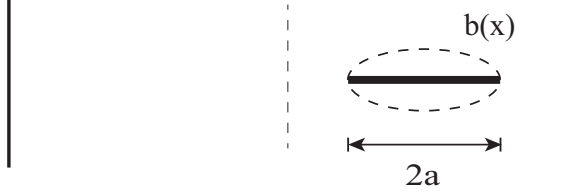
Case 1:  $e = 0$ Case 2:  $e = 0.5$ 

Figure 10: Illustration of two crack cases

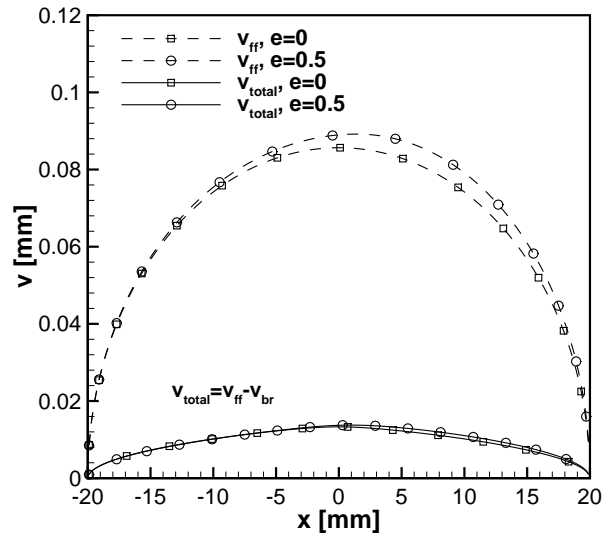


Figure 11: Comparison of crack opening displacements

$$K_{total} = K - K_{br} \quad (49)$$

The key to analyse the failure in such fibre-reinforced aluminum panels is to resolve the load transfer between the cracked metal layers and the intact bridging fibre layers with the concept of displacement compatibility. The displacement of the cracked metal layers and the elongation of the bridging fibres should be compatible at the delamination front. This displacement compatibility is given in a simplified form without considering the shear deformation of the fibre prepreg:

$$v_{ff}(x) - v_{br}(x) = \frac{S_f(x) + S_{br}(x)}{E_f} b(x) \quad (50)$$

where  $x$  denotes the location along the crack flank with the origin at the middle of the crack,  $v_{ff}$  is the crack opening in the metal layer due to the far-field applied load,  $v_{br}$  is the crack closing due to the bridging stress distribution,  $S_{br}(x)$ . The right side of Eq. 50 is the fibre elongation. It is evident that  $S_{br}$  is the resultant stress due to the load transfer from cracked metal layer into the intact fibre layers [5, 18].

Implementing Eq. 50 requires discretization of the delamination shape into bar-elements. For the current study, the bar width of 0.2 mm is considered, see Fig. 12. Model 3 is applied to calculate both the  $v_{ff}(x)$  and the  $K_1$  and  $K_2$  for the two cases. The stress in the metal layers ( $S_m$ ) due to the far-field load is used for

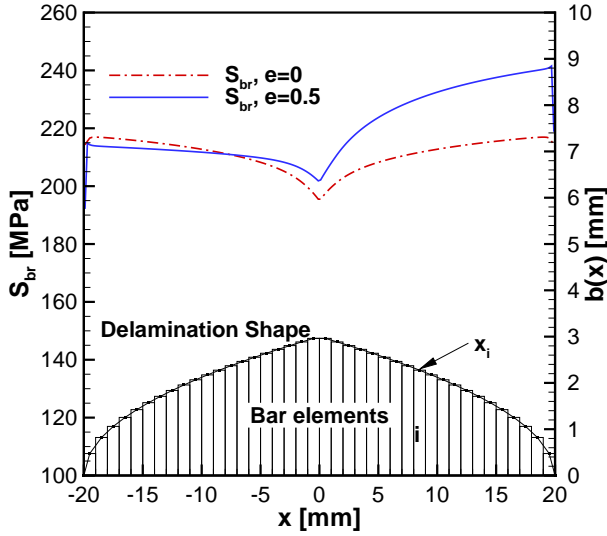


Figure 12: Delamination shape and  $S_{br}$

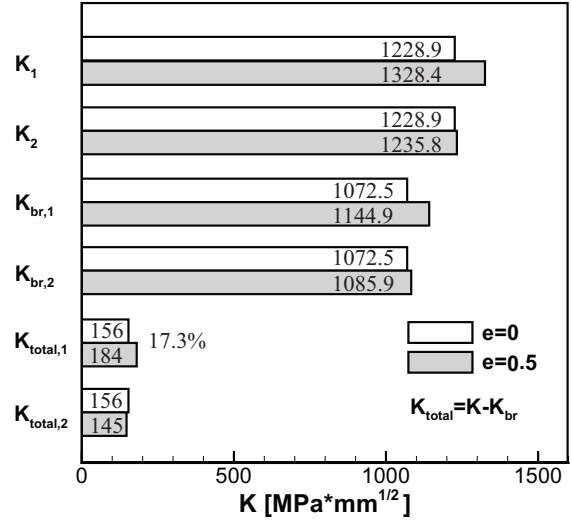


Figure 13: Comparison of stress intensity factors

250 the calculation.  $S_m = 151.9 \text{ MPa}$  and  $S_f = 21.95 \text{ MPa}$  are calculated with the Classic Laminate Theory [19]. The Westergaard stress function for point loads on a crack on Page 5.6 in the handbook [7] is applied to calculate the  $K_{br}$  and  $v_{br}$ . Detailed calculation procedure can be found in [20].

255 The procedure for calculating the bridging stress distribution has been well established by Alderliesten [5, 18]. Since it is not the focus of this paper, the detailed calculation procedure can be found in [5, 18, 20], only the results are presented. The results of the crack openings are presented in Fig. 11. The obtained  $S_{br}$  for each crack case is presented in Fig. 12. The  $K$  results are presented in Fig. 13

260 Since the delamination is at the interface between isotropic aluminium and orthotropic fibre layer, calculating strain energy release rate,  $G$ , at the delamination tip is much easier than calculating Mode II stress intensity factor [18].  $G$  can be used to characterize the delamination propagation [20]. A detailed calculation of non-symmetric crack growth and accompanying delamination propagation in Glare under fatigue loading has been reported in [20].

### 5.2. Significance of the COD of a non-symmetric crack

265 The above example shows how the opening displacement solution can be applied to analyse the failure in built-up structures. It is noticeable that analysing the COD of non-symmetric cracks in such structures is quite indispensable. The increment in the opening displacement and the non-symmetric opening configuration, as shown in Fig. 11, lead to a quite difference in the load transferred between the intact stiffening elements and the cracked panel. The difference is larger for the critical crack tip, see Fig. 12. The maximum bridging stress for the non-symmetric crack is 11.3% higher than that for the symmetric crack.

270 Even though the larger load transfer occurs for the non-symmetric crack case, the resultant stress intensity factor for crack tip 1 ( $K_{total,1}$ ) of Case 2 is still 17.3% higher than that of Case 1. Besides, this larger load transfer between the cracked metal layer and intact fibre layers could result in larger delamination under fatigue loading in reality, further reducing the load bearing capability of the structure. Neglecting the non-symmetry effects due to a non-symmetric crack in such a thin-walled structure with stiffening elements can result in a non-conservative prediction, which must be avoided for safety critical structures.

275 It is evident now that the interaction between a cracked panel and its stiffening elements is crucial in determining the failure. This interaction can be easily analysed with the COD solution and the concept of displacement compatibility, as described in the preceding subsection. The changes in the opening displacement due to non-symmetry have to be accounted in the analysis. A remarkable consequence of this

analytical solution is to circumvent the burden of developing computationally consuming FEM models. This advantage emerges when fatigue problems in built-up structures need to be addressed.

## 6. Conclusion

This paper develops analytical models to estimate the deformation behaviour in eccentrically cracked panels. The Westergaard stress function is simplified to calculate the opening displacement in the crack and the stress distributions ahead of two crack tips. The stress intensity factor solutions arising from the proposed models are compared to analytical results from Isida. Based on the validation, Model 3 provides good estimations of both the crack opening displacement and stress intensity factors of a non-symmetric crack. Back calculating Isida  $\beta$  factors could provide very accurate crack opening displacement predictions for non-symmetric cracks.

It is found that the crack length for a non-symmetric crack should be defined as the length from the maximum crack opening location to the crack tip in the context of the Westergaard stress distribution. The load is preferably transferred by one or another ligament in an eccentrically cracked panel as a result of the stiffness difference in the ligament. The Westergaard stress distribution in front of the crack tip is a valid assumption.

The deformation solution of eccentrically cracked panels obtained from this paper is essential in analysing failure in built-up structures containing non-symmetric cracks. The increment in the opening displacement due to the non-symmetry deteriorates the stress state of the bridging elements. Neglecting this part could lead to nonconservative design of stiffening elements for thin-walled structures. The analytical COD solutions are very simple to use together with the concept of displacement compatibility in analysing failure in thin-walled panels with stiffening elements.

## Acknowledgement

The authors gratefully acknowledge the Chinese Scholarship Council (CSC) for financial support.

## References

- [1] P. M. Toor, A review of some damage tolerance design approaches for aircraft structures, *Engineering Fracture Mechanics* 5 (4) (1973) 837–880.
- [2] T. Swift, Fracture analysis of adhesively bonded cracked panels, *Journal of Engineering Materials and Technology* 100 (1) (1978) 10–15, 10.1115/1.3443441.
- [3] J. Schijve, Crack stoppers and arall laminates, *Engineering Fracture Mechanics* 37 (2) (1990) 405–421.
- [4] M. Heinimann, R. Bucci, M. Kulak, M. Garratt, Improving damage tolerance of aircraft structures through the use of selective reinforcement, in: *Proceedings of the 23rd symposium of international committee on aeronautical fatigue, ICAF 2005, Hamburg, 2005*, pp. 197–208.
- [5] R. C. Alderliesten, Analytical prediction model for fatigue crack propagation and delamination growth in glare, *International Journal of Fatigue* 29 (4) (2007) 628–646.
- [6] C. Rans, R. Rodi, R. Alderliesten, Analytical prediction of mode I stress intensity factors for cracked panels containing bonded stiffeners, *Engineering Fracture Mechanics* 97 (0) (2013) 12–29.
- [7] H. Tada, P. C. Paris, G. R. Irwin, *The stress analysis of cracks handbook*, ASME, New York, 2000.
- [8] T. Hiroshi, A note on the finite width corrections to the stress intensity factor, *Engineering Fracture Mechanics* 3 (3) (1971) 345–347.
- [9] D. L. Ball, The development of mode I, linear-elastic stress intensity factor solutions for cracks in mechanically fastened joints, *Engineering Fracture Mechanics* 27 (6) (1987) 653–681.
- [10] W. Qizhi, The crack-line stress field method for analysing sifs of strips-illustrated with an eccentrically cracked tension strip, *International Journal of Fracture* 59 (2) (1993) R39–R43.
- [11] D. L. Chen, B. Weiss, R. Stickler, A new approach for the determination of stress intensity factors for finite width plate, *Engineering Fracture Mechanics* 48 (4) (1994) 561–571.
- [12] M. Isida, Stress-intensity factors for the tension of an eccentrically cracked strip, *Journal of Applied Mechanics* 33 (3) (1966) 674–675, 10.1115/1.3625138.
- [13] H. Westergaard, Bearing pressure and cracks., *Journal of Applied Mechanics* 6 (1939) 49–53.
- [14] E. E. Gdoutos, *Fracture mechanics : an introduction*, 2nd Edition, Springer, Dordrecht, the Netherlands, 2005.
- [15] I. Barsoum, K. S. Ravi Chandran, Stress intensity factor solutions for cracks in finite-width three layer laminates with and without residual stress effects, *Engineering Fracture Mechanics* 70 (15) (2003) 2015–2031.

- 330 [16] K. S. Ravi Chandran, I. Barsoum, Determination of stress intensity factor solutions for cracks in finite-width functionally graded materials, *International Journal of Fracture* 121 (3-4) (2003) 183–203.
- [17] B. Cotterell, A. G. Atkins, A review of the  $J$  and  $I$  integrals and their implications for crack growth resistance and toughness in ductile fracture, *International Journal of Fracture* 81 (4) (1996) 357–372. doi:10.1007/BF00012428.  
URL <https://doi.org/10.1007/BF00012428>
- 335 [18] R. C. Alderliesten, Fatigue crack propagation and delamination growth in glare, Ph.D. thesis, Delft University of Technology, Delft, the Netherlands (2005).
- [19] J. J. Homan, Fatigue initiation in fibre metal laminates, *International Journal of Fatigue* 28 (4) (2006) 366–374.
- [20] W. Wang, C. Rans, R. Benedictus, Analytical prediction model for non-symmetric fatigue crack growth in fibre metal laminates, *International Journal of Fatigue* 103 (2017) 546–556.